Shear Wave Speed and Dispersion Measurements Using Crawling Wave Chirps

Zaegyoo Hah[1], Alexander Partin[1], and Kevin J. Parker[1]

Abstract

This article demonstrates the measurement of shear wave speed and shear speed dispersion of biomaterials using a chirp signal that launches waves over a range of frequencies. A biomaterial is vibrated by two vibration sources that generate shear waves inside the medium, which is scanned by an ultrasound imaging system. Doppler processing of the acquired signal produces an image of the square of vibration amplitude that shows repetitive constructive and destructive interference patterns called "crawling waves." With a chirp vibration signal, successive Doppler frames are generated from different source frequencies. Collected frames generate a distinctive pattern which is used to calculate the shear speed and shear speed dispersion. A special reciprocal chirp is designed such that the equi-phase lines of a motion slice image are straight lines. Detailed analysis is provided to generate a closed-form solution for calculating the shear wave speed and the dispersion. Also several phantoms and an ex vivo human liver sample are scanned and the estimation results are presented.

Introduction

Over the last 20 years, there has been significant innovation in the area of imaging the elastic properties of tissue. Numerous techniques have been used to image the mechanical properties of biomaterials, including vibration elastography imaging, compression elastography, magnetic resonance elastography, shear wave imaging, vibro-acoustic spectroscopy, acoustic radiation force imaging (ARFI), crawling waves, and spatially modulated ultrasonic radiation force (SMURF).[1] The imaging can be static where the applied force is in the form of a step-function, or dynamic with the applied force either in continuous or impulse shape.[1,2] While many of these techniques assume that shear modulus and shear speed are practically constant, recent research illustrates the importance of changes in the elastic properties of tissue over a given frequency range and the dispersion of shear wave speed.[3-6]

[1]Department of Electrical and Computer Engineering, University of Rochester, Rochester, NY, USA

Corresponding Author:
Kevin J. Parker, Department of Electrical and Computer Engineering, University of Rochester, Hopeman Building 203, P.O. Box 270126, Rochester, NY 14627-0126, USA.
Email: kevin.parker@rochester.edu

It is understood that increasing amounts of fat in the normal liver will increase the dispersion (i.e., the frequency dependence or slope) of the speed and attenuation of shear waves, while slightly reducing the speed of sound. This is simply the consequence of adding a viscous (and highly lossy) component to the liver, which otherwise would exhibit a strong elastic component with lower dispersion.[3,7,8] Using a variety of techniques, different groups have examined shear wave dispersion in tissues and pathologies, including breast cancer,[9] liver fibrosis,[10] muscle,[11,12] normal mammalian livers,[11] and gelatins.[13]

In an attempt to optimize measurement time (compared with tone burst techniques) and signal-to-noise ratio (compared with radiation force techniques), it would be advantageous to use chirps sweeping over a frequency range using external shear wave sources.

The resultant shear motion of the biomaterial is detected by Doppler scanning of the medium at a given frame rate. The acquired elasticity patterns over time—called "elasticity movies"—will be further analyzed to determine the shear speed and the dispersion. A specific chirp is designed for this purpose to facilitate more efficient and robust post-processing. This is important in that the design of the chirp dictates the shape of each of the frame images which, in turn, allows for flexibility in processing the acquired data. The next section describes theoretical details of the interference patterns using two external sources, a distinctive "motion slice" from elasticity movies, design of a specific chirp signal, and calculating the shear speed dispersion using chirp signals. Also, some experimental results of some phantoms and a liver specimen are presented.

Theory

Interference Pattern

When a homogeneous biomaterial is vibrated by two separate sources each vibrating at the same frequency, an interference pattern is generated within the medium. The pattern comes from the repetitive constructive and destructive interference between two waves traveling in the opposite direction. As shown in Figure 1, two vibration sources, vibrating at f_v and located at $x = 0$ and $x = D$, respectively, generate shear waves into a biomaterial with a initial phase difference φ. The waves interfere and result in particle motions that are dependent on the location relative to the sources. Additional configuration of sources more suitable for in vivo experiments is described in Partin et al.[14]

The shear wave interference pattern can be detected by using an ultrasound probe that transmits a series of scanning pulses along a scan line and receives echoes along the same line. The acquired data are then processed using Doppler processing to produce the measure of vibration amplitude at each point of the region of interest. A detailed derivation of the interference pattern can be found in Hah.[15] From a superposition of two interfering plane waves, the resulting image of the interference pattern $P(x, \varphi)$ would be

$$P(x, \varphi) \quad = 2A^2 e^{-\alpha D} \cosh\left[2\alpha\left(x - \frac{D}{2}\right)\right] \quad + 2A^2 e^{-\alpha D} \cos\left[2k\left(x - \frac{D}{2}\right) + \varphi\right], \tag{1}$$

$$= \qquad \text{baseline term} \qquad + \qquad \text{oscillating term}$$

where A is the amplitude of the vibrating signal, α is the shear wave attenuation coefficient, k is the wave number of shear wave, and φ is the initial phase difference. A typical pattern is displayed in Figure (2a) with a profile at a given depth in Figure (2b) where the baseline and oscillating terms can be clearly discriminated. Therefore, if we have two patterns at $\varphi = \varphi_0$ and $\varphi = \varphi_0 + \pi$, respectively, but at the same vibration frequency, the baseline term would be
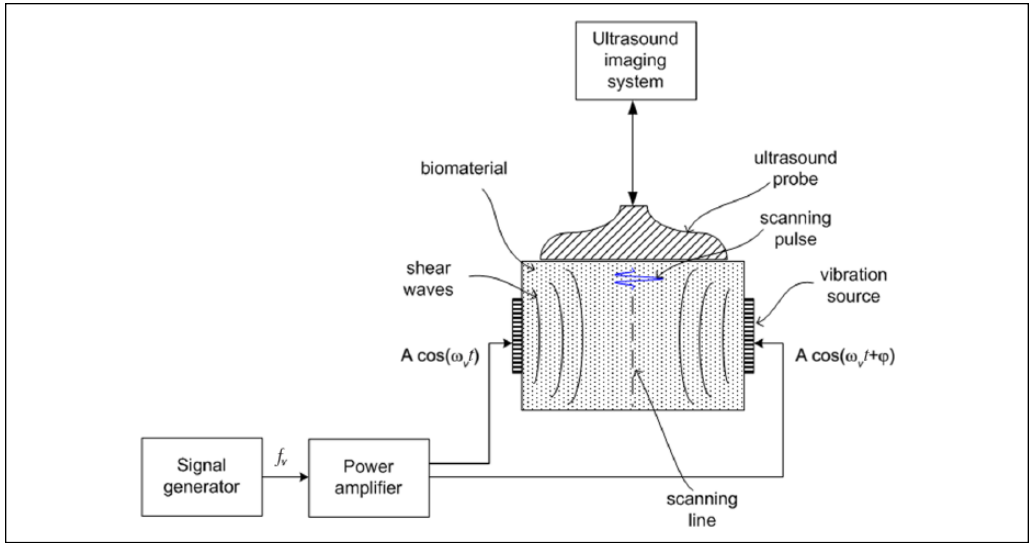
Figure 1. A block diagram showing the basic configuration of measurement setup for measuring shear speed and dispersion.
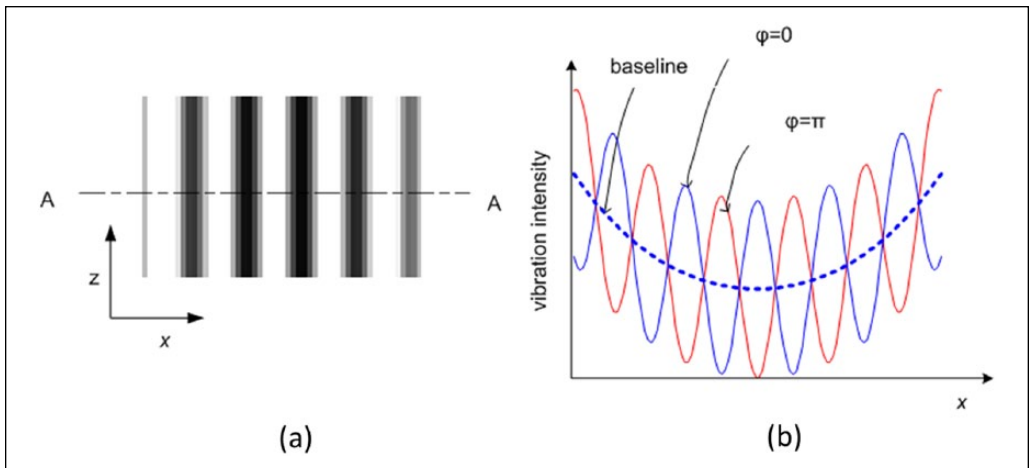

Figure 2. A typical interference pattern (a), and the profile at a constant depth, line A–A, (b). Two interference pattern obtained with initial phase difference of π would cancel each other to leave only the baseline. Removing the baseline would produce the oscillating term.

$$\text{baseline term} = \frac{P(x, \varphi_0) + P(x, \varphi_0 + \pi)}{2} \tag{2}$$

and the oscillating term would be

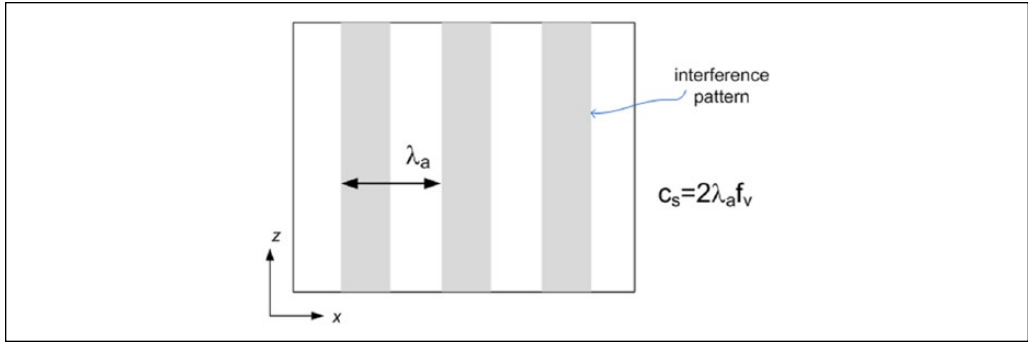$$\text{oscillating term} = P(x, \varphi_0) - \text{baseline term}. \tag{3}$$

Figure 3. An interference pattern with baseline removed. Apparent wavelength can be measured and the shear speed can be calculated.

The sinusoidal fluctuation of the oscillating term is indicative of the medium properties because, as illustrated in Figure 3, the apparent wavelength λ_a for the shear wave c_s can be extracted and the shear wave can be calculated as

$$c_s = 2\lambda_a f_v. \tag{4}$$

Shear Speed Dispersion with a Linear Chirp

If we want to measure the shear speed dispersion of a homogeneous media, we can generate a series of interference patterns over a defined frequency range, calculate the shear speed at each frequency, and calculate the slope of shear speed as a function of frequency. However, this approach is slow and, especially in the presence of noise, the slope measurement can have a large uncertainty. At the same time, at low frequencies in a biomaterial with a high shear speed, the wavelength is large and there may not be enough number of oscillations across the aperture thereby rendering the measured λ_a quite uncertain. Therefore, it would be more advantageous to employ a method where, instead of doing frame-by-frame analysis, the entire set of measured data is integrated and collectively analyzed.

Instead of vibrating the medium at a constant frequency, the medium can be vibrated by a simple linear chirp, shown in Figure 4, where the vibration frequency $f(t)$ changes from f_0 to f_1 over the duration T:

$$f(t) = f_0 + (f_1 - f_0)\frac{t}{T}, 0 \leq t \leq T. \tag{5}$$

In this case, for a fixed frame rate, each frame will display an interference pattern specific to the vibration frequency of the frame as illustrated in Figure 5. As time increases, the vibration frequency would increase, and because the wavelength of the interference pattern would decrease, more interference stripes will be observed. Moreover, if we take a slice of the data defined in Figure 5 as dotted lines (we refer to this orientation of data as a motion slice) at a fixed depth (z) having time (or frame number) on one axis and horizontal distance (x) on the other, the motion slice image would look like that shown in Figure 6. The distance between the adjacent stripes equals the apparent wavelength of the interference pattern λ_a and, because λ_a is inversely proportional to the vibration frequency, the equi-phase line would be in the form of a hyperbola as shown in Figure 6. The equi-phase lines can be obtained by several methods, including (1) by tracking the local maxima
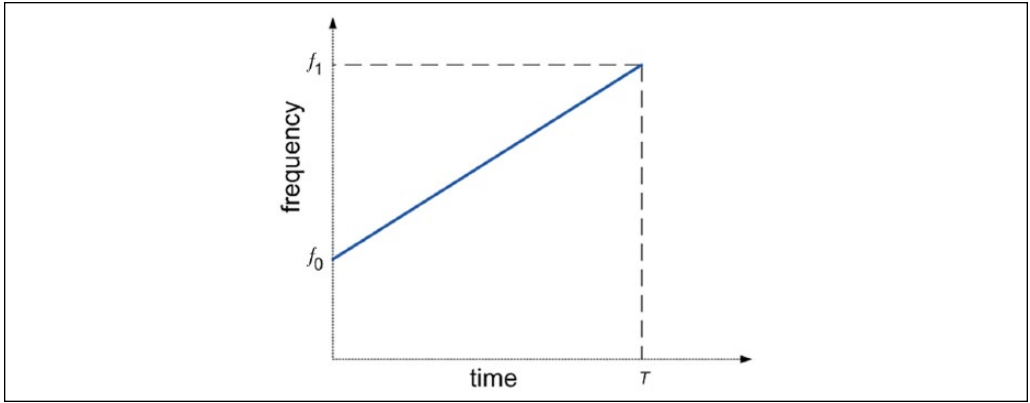
Figure 4. A linear chirp of Equation (5). The vibration frequency $f(t)$ changes from f_0 to f_1 over the duration T.
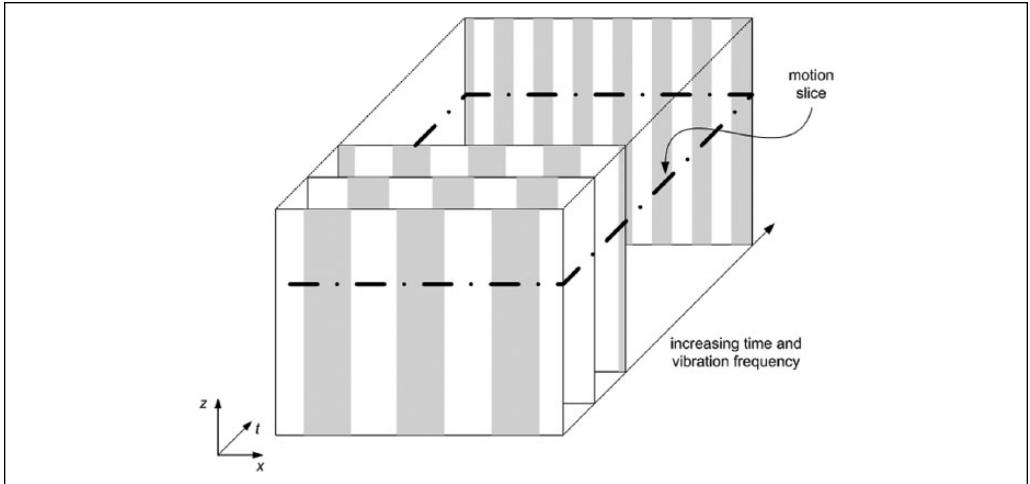

Figure 5. A multiple frame data obtained with a linear chirp.
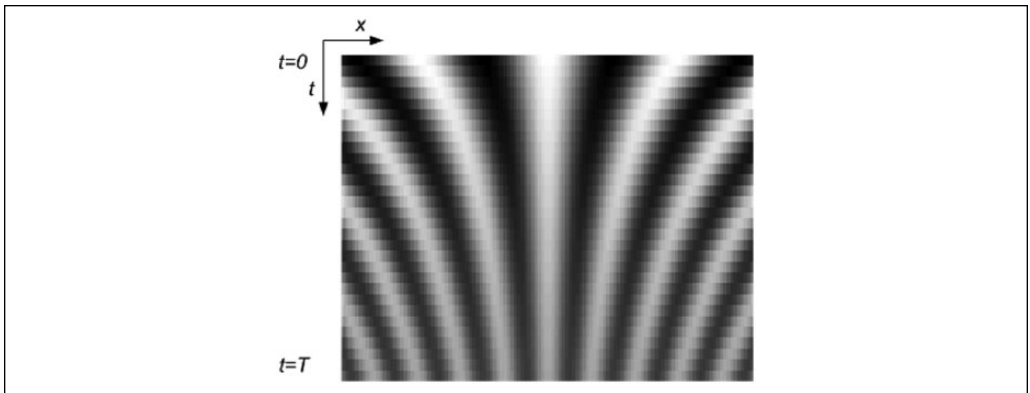

Figure 6. A motion slice image obtained with a linear chirp shown in Figure 4.
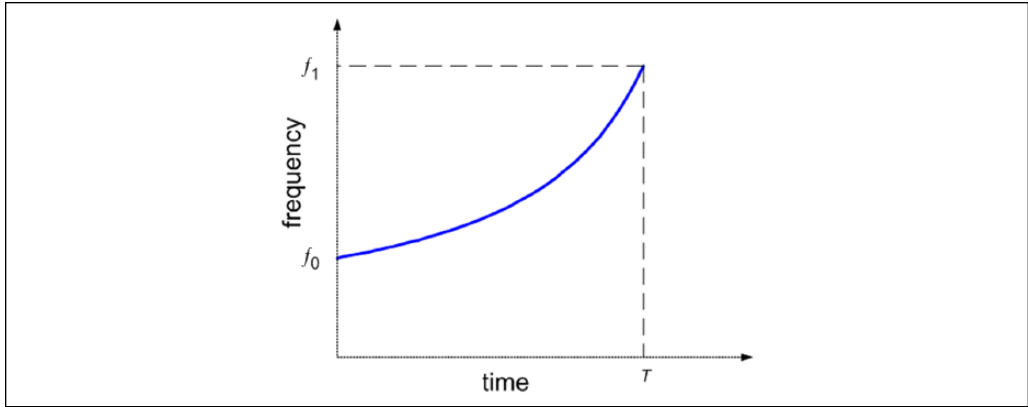
Figure 7. A reciprocal chirp given by Equation (6).

or minima of the oscillating terms for each frequency; (2) by first normalizing the oscillating terms for each frame, and then tracking the line of minimal variance at each point in the motion slice image; and (3) by converting the oscillation term into a phase domain using a Hilbert transform, and then tracking the line of minimal variance at each point in the motion slice image.

A Reciprocal Chirp

A specific chirp pattern better suited for the analysis of a motion slice can be designed as

$$ f(t) = \frac{f_0 f_1}{\left[f_1 + (f_0 - f_1)\dfrac{t}{T} \right]}. \tag{6}$$

This chirp, as illustrated in Figure 7, can be scanned either continuously as shown in Figure (8a) or stepwise as shown in Figure (8b). The step durations in Figure (8b) are consistent with Doppler frame rates, typically 10/s in our system. The amplitude of the chirp can also be modulated to compensate for system effects, so as to produce a more uniform response over the frequency range.

If the shear speed of a biomaterial is constant at c_0, then the apparent wavelength for this chirp would be

$$
\begin{aligned}
\lambda_a(t) \quad &= \frac{c_0}{2 f(t)} \\
&= \frac{c_0 \left[f_1 + (f_0 - f_1)\dfrac{t}{T} \right]}{2 f_0 f_1} \\
&= \frac{c_0}{2 f_0} + \frac{c_0 (f_0 - f_1)}{2 f_0 f_1 T} t.
\end{aligned} \tag{7}
$$

This means that the motion slice image obtained with the reciprocal chirp is quite different from the one with the linear chirp. As shown in Figure 9, the image is no longer a hyperbolic
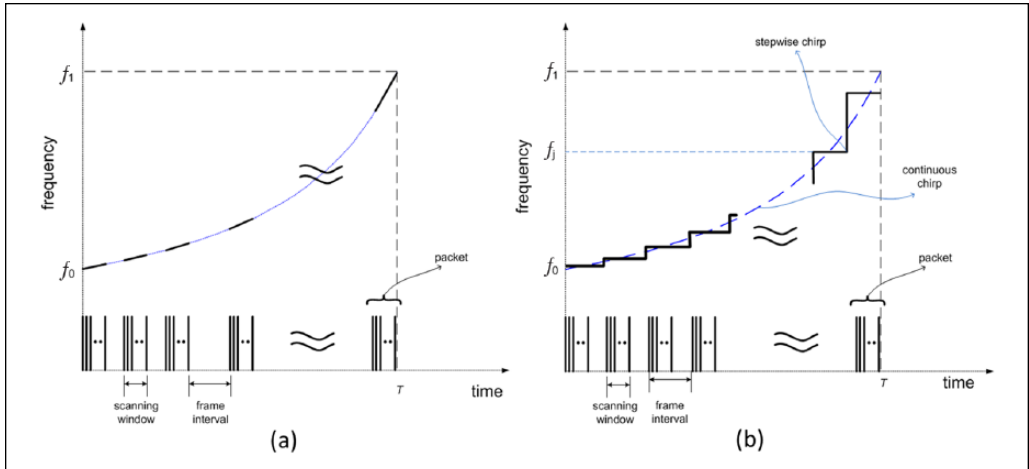
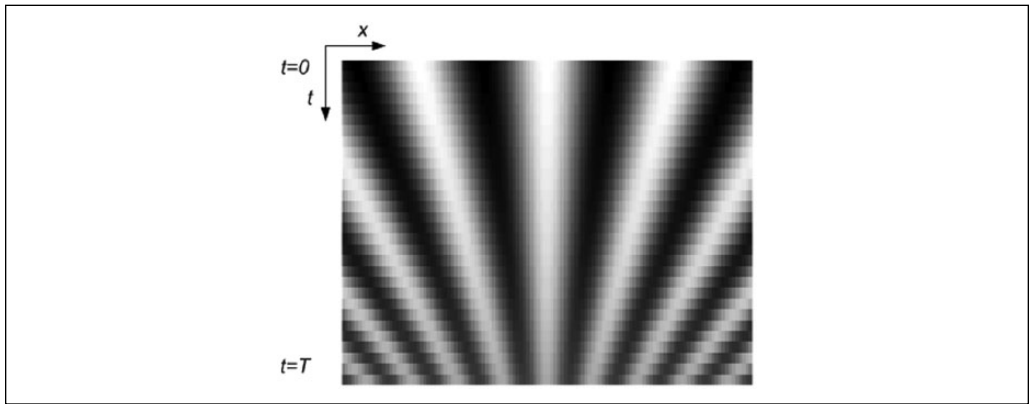**Figure 8.** Scanning diagrams for the reciprocal chirp: a continuous (a) and a stepwise (b) scanning.

Figure 9. A motion slice image obtained with the reciprocal chirp of Equation (6) and Figure 7. The equi-phase lines are straight lines.

shape of Figure 6. Instead, the equi-phase lines are straight lines. This feature facilitates further smoothing and collective processing not available with the linear chirp of Figure 4.

Shear Speed Dispersion

As a first-order linear approximation over a limited bandwidth, we consider a homogeneous bio-material with a constant shear speed dispersion γ over the frequency range of $[f_0, f_1]$, that is,

$$\gamma = \frac{dc_s}{df}, \tag{8}$$

then the shear speed from the reciprocal chirp would be

$$c_s(t) = c_0 + \gamma \left[f(t) - f_0 \right], \tag{9}$$

where c_0 is the shear speed at f_0. The units of γ are in meters but as a convenient reminder of its nature as a slope $\Delta c/\Delta f$, we also use m/s/Hz or m/s per 100 Hz. The apparent wavelength would be

$$
\begin{aligned}
\lambda_a(t) &= \frac{c_s(t)}{2f(t)} \\
&= \frac{c_0 + \gamma\left[f(t) - f_0\right]}{2f(t)} \\
&= \frac{c_0 + \gamma\left[\dfrac{f_0 f_1}{f_1 + (f_0 - f_1)\dfrac{t}{T}} - f_0\right]}{2\dfrac{f_0 f_1}{f_1 + (f_0 - f_1)\dfrac{t}{T}}} \\
&= \frac{c_0}{2f_0} + \frac{(f_0 - f_1)(c_0 - \gamma f_0)}{2f_0 f_1 T}t.
\end{aligned}
\tag{10}
$$

The motion slice, therefore, will still show straight equi-phase lines. Moreover, the equi-phase lines intersect at the same point, $t = t_0$, as illustrated in Figure 10 such that

$$
t_0 = \frac{f_1 T}{(f_1 - f_0)\left(1 - \dfrac{\gamma f_0}{c_0}\right)},
\tag{11}
$$

and the center angle between the adjacent equi-phase lines is given by

$$
\tan(\theta_0) = \frac{(f_1 - f_0)(c_0 - \gamma f_0)}{2f_0 f_1 T}.
\tag{12}
$$

Moreover, the speed dispersion introduces changes to t_0 and θ_0 as displayed in Figure 11: with increasing dispersion γ, t_0 increases and θ_0 decreases. Therefore, the four variables, c_0 (the shear wave speed at f_0), γ (dispersion of speed), θ_0 (angle of adjacent equi-phase line defined in Equation (12)), and t_0 (time-intersect defined in Equation (11)) are combined. And, if we measure θ_0 and t_0, c_0 and γ will follow:

$$
c_0 = 2f_0 t_0 \tan(\theta_0)
\tag{13}
$$

and

$$
\gamma = 2\tan(\theta_0)\left[t_0 - \frac{f_1 T}{(f_1 - f_0)}\right].
\tag{14}
$$

Two parametric diagrams are shown in Figures 12 and 13 for c_0 (shear speed at f_0) and γ (shear speed dispersion) for an exemplary case of f_0 (start frequency) = 100 Hz, f_1 (stop frequency) = 300 Hz, and T (sweep duration) = 3 s. From the measured θ_0 and t_0 pair, the
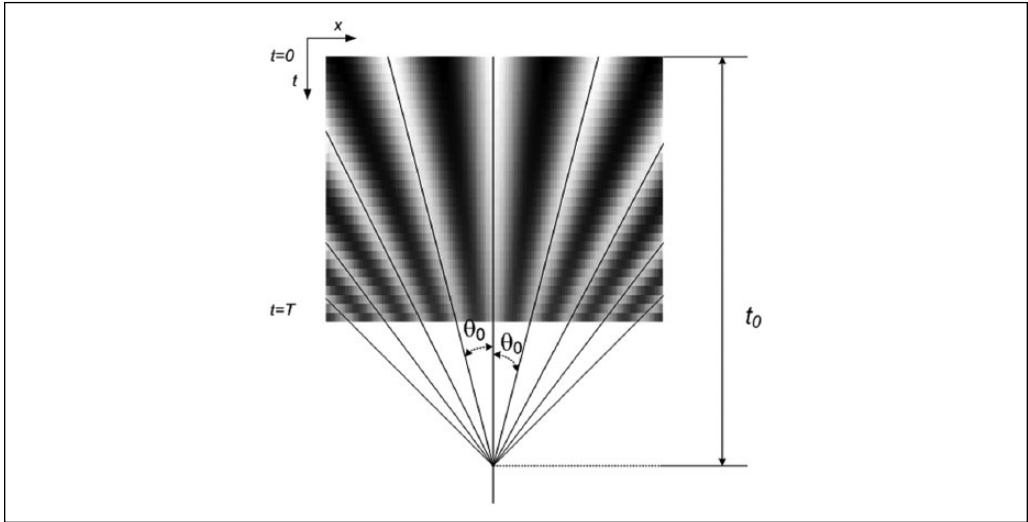
Figure 10. A graphic illustration explaining the concept of the time-intersect and the center angle between the adjacent equi-phase lines.
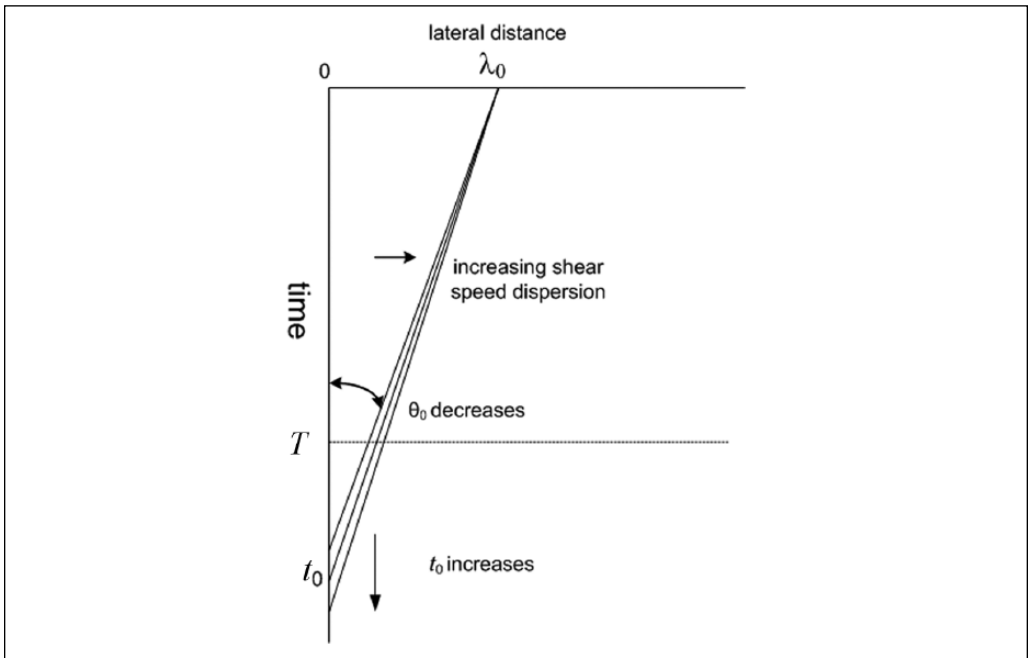

Figure 11. A diagram showing the effect of increasing shear speed dispersion on the time-intersect t_0 and the center angle θ_0.

corresponding c_0 and γ can be calculated. For example, if $\theta_0 = 0.002$ m/s and $t_0 = 5.318$ s then $c_0 = 2.127$ m/s and $\gamma = 0.0033$ m/s/Hz = 0.33 m/s per 100 Hz as the point p in Figures 12 and 13 illustrates.
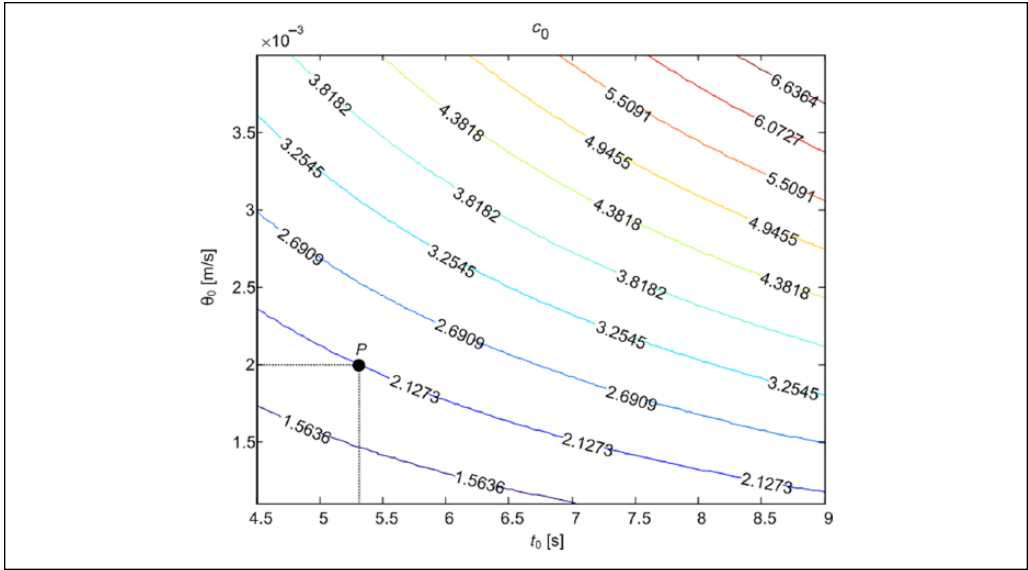
Figure 12. A parametric plot of the shear wave speed from the measured time-intersect and the angle between the adjacent equi-phase lines.
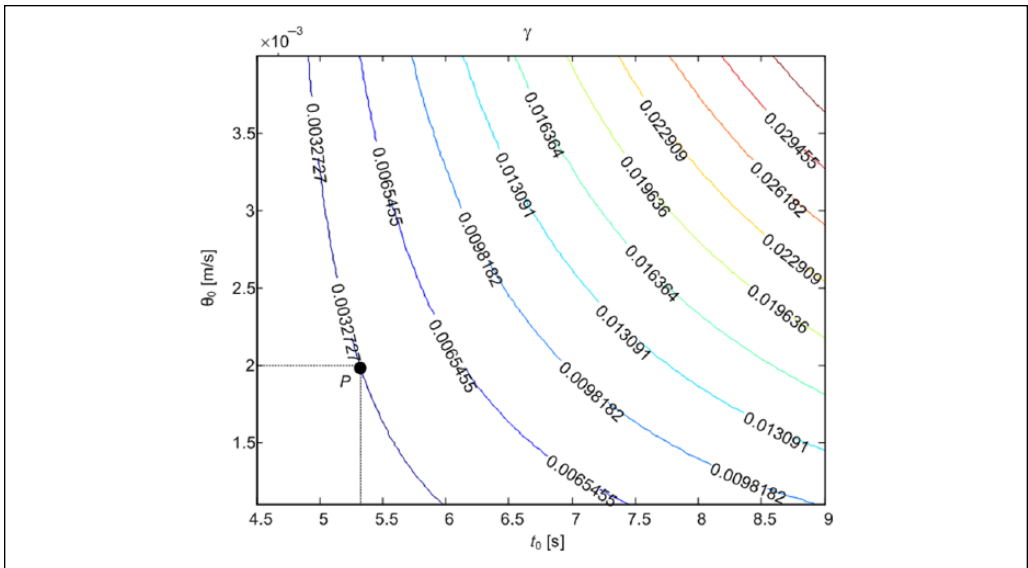

Figure 13. A parametric plot of the shear wave speed dispersion from the measured time-intersect and the angle between the adjacent equi-phase lines.

Method

Several samples were prepared and scanned for experimental verifications: two gelatin phantoms (9.25% and 13.4%), a castor oil (18.5%) phantom, and an ex vivo human liver sample. To fabricate a 9.25% gelatin phantom, 185.4 g gelatin (300 Pork Bloom Gelatin; Gelatin Innovation Inc.,

Schiller Park, IL, USA), 16.2 g NaCl, and 2.7 g agar (Difco Agar Technical Solidifying Agent, BD, Sparks, MD, USA) were added to 1.8 L deionized water. The mixture was then heated to 55°C using a microwave until most of the solid was dissolved. It was further stirred and cooled using a magnetic mixer to approximately 30°C. The cooled mixture was poured into a $4 \times 5 \times 6$ inch cube-shaped mold and refrigerated at 4°C overnight. The 13.4% gelatin phantom was similarly made with 281.5 g of gelatin with the other ingredients kept at the same level. The castor oil phantom was made of 1.8 L deionized water, 180 g gelatin, 460 g castor oil (Castor Oil–Refined, SoapGoods.com, Atlanta, GA, USA), 16.2 g NaCl, 2.7 g agar, and 27 g surfactant (Liquid UltraIvory®, Procter & Gamble Co., Cincinnati, OH, USA). The mixture was stirred gently to avoid introducing air bubbles while forming a uniform emulsion. A human liver ex vivo sample was also prepared. The liver was from a 50-year-old patient who died of a stroke and the liver sample was excised less than 24 hours after death following the guidelines of University of Rochester Institutional Review Board. The liver sample, about $5 \times 2 \times 6$ cm^3, was embedded in a 9.25% gelatin phantom for scanning.

Each sample was scanned by a GE LOGIQ E9 imaging system (GE Healthcare, Wauwatosa, WI, USA) stepwise simulating the scanning sequence depicted in Figure (8b) with f_0 = 110 Hz, f_1 = 300 Hz, and the duration of each step was T = 3 s at 15 different frequencies: 110, 115, 121, 127, 134, 142, 151, 161, 172, 186, 201, 219, 241, 267, and 300 Hz. Because this is a clinical scanner and not programmable under our control, the acquisition resembled the sequence of Figure (8b), with discrete steps due to the need for manual restart of the data collection at each frequency step. The shear waves were generated using mechanical vibration sources (Brüel and Kjaer Model 4810, Naerum, Denmark) positioned at the opposite sides of the phantom. The frequency response of the sources is flat over the frequencies used in our experiments. The temperature of the phantom during scanning was 20°C for 9.25% gelatin, 18.5°C for 13.4% gelatin, 18°C for the castor oil phantom, and 14°C for the liver sample. Four acquired frames of gelatin 9.25% phantom are shown in Figure 14 at 110, 134, 186, and 300 Hz as an example at a region of interest (ROI) depth around 2.5 cm. The acquired data were processed following the theory described in the previous section.

Results

The analysis of the 9.25% gelatin phantom is shown in Figure (15a). The time-intersect t_0 was measured at 4.66 s and the tangent of the center angle was 0.0047, which produced c_0 = 3.09 m/s and γ = 7.0×10^{-5} m/s/Hz. Similarly processed results for the 13.4% gelatin phantom and the castor oil phantom are also shown in Figure (15b) and (c) with c_0 = 4.27 m/s and γ = 8.9×10^{-4} m/s/ Hz, and c_0 = 4.37 m/s and γ = 1.5×10^{-3} m/s/Hz, respectively. The human liver sample data were also processed to produce c_0 = 2.55 m/s and γ = 5.1×10^{-3} m/s/Hz as shown in Figure 15(d). The liver sample was inspected by a pathologist in parallel and reported to have 30% fat. The shear speed dispersion for the gelatin phantoms is very small and can be neglected if the frequency range of interest is small (several hundred Hz). However, the castor oil phantom shows higher dispersion as expected from theory and from previous results using crawling waves.[5] The increase of the speed dispersion is attributed mainly to the viscosity introduced by castor oil into the gelatin–water matrix. The same reasoning can be made for the high value of dispersion for the liver sample. Furthermore, the liver dispersion value which can be restated as γ = 0.51 m/s per 100 Hz is similar to the 35% steatotic liver reported in Barry et al.[5]

It should be noted that all elastic properties of the test samples are sensitive to temperature and so are shear speed and dispersion. This means that a phantom of the same composition would show different shear speed and dispersion as a function of temperature. Also, in this study, there was a slight increase of the phantom temperature during the scanning from
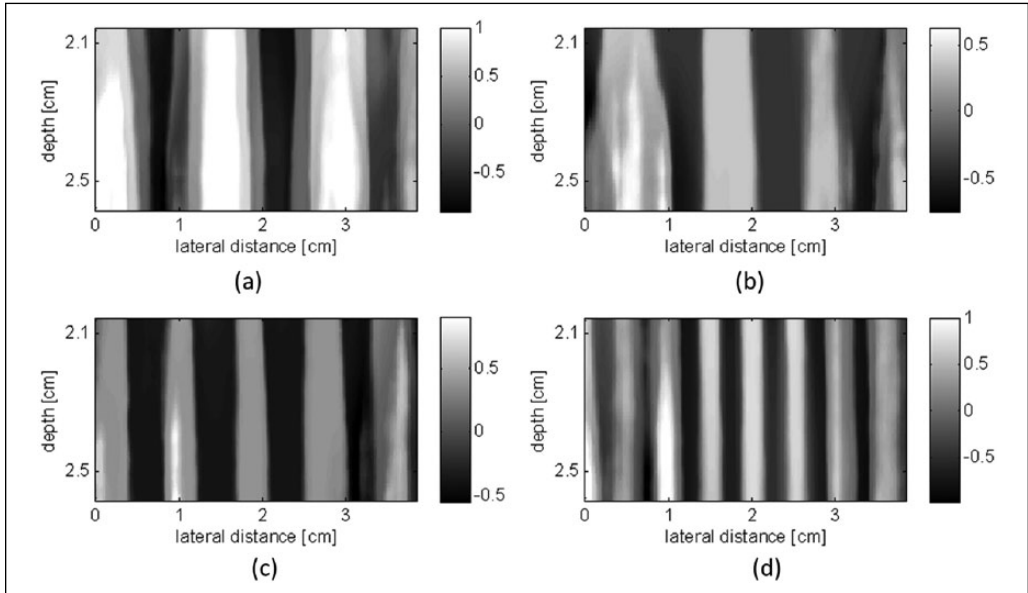
Figure 14. Interference patterns of gelatin 9.25% phantom at (a) 100 Hz, (b) 134 Hz, (c)186 Hz, and (d) 300 Hz. The scanning was performed stepwise simulating the scanning sequence depicted in Figure 8b.

ultrasound energy absorbed in the phantom, thermal conduction from the ultrasound probe, and change of the room temperature; however, the temperature change was less than 0.7°C, small enough to be neglected.

Discussion and Conclusion

A novel approach for measuring shear speed and shear speed dispersion of elastic materials is described with accompanying experimental data and results. Biomaterials were scanned while being vibrated with a reciprocal chirp signal over the defined range such that each frame of the acquired movie represents one frequency. The motion slice defined at a certain depth will then display distinctive straight equi-phase lines that facilitate further processing.

This approach of sweeping the vibration frequency and the analysis thereof provides some advantages over earlier techniques where repetitive measurements are made for each frequency at discrete steps over a bandwidth. The collective analysis of the measured frames allows a more robust signal processing and the measurement of the shear wave speed and the speed dispersion, thereby improving accuracy. The lower limit of acquisition time will depend on a number of factors, including the size of the region of interest, the spatial sampling, the Doppler packet size, and the Doppler signal-to-noise ratio. Therefore, it is difficult to generalize. However, in an integrated approach with control of the continuous reciprocal chirp and the scanner, the measurement time to cover the required frequency range would decrease considerably compared with time-consuming alternatives that capture a series of discrete shear wave frequencies as distinct acquisitions. The analysis of the samples in this study was found to be relatively insensitive to the choice of depth of the motion slice. This is because the parallel source configuration of Figure 1 for samples leads to interference patterns that are nearly plane and vertical within the field of view (see Figure 14 for examples). Thus, the motion slice images formed are highly correlated over many centimeters of depth within the imaging ROI. However, the configuration of Figure 1
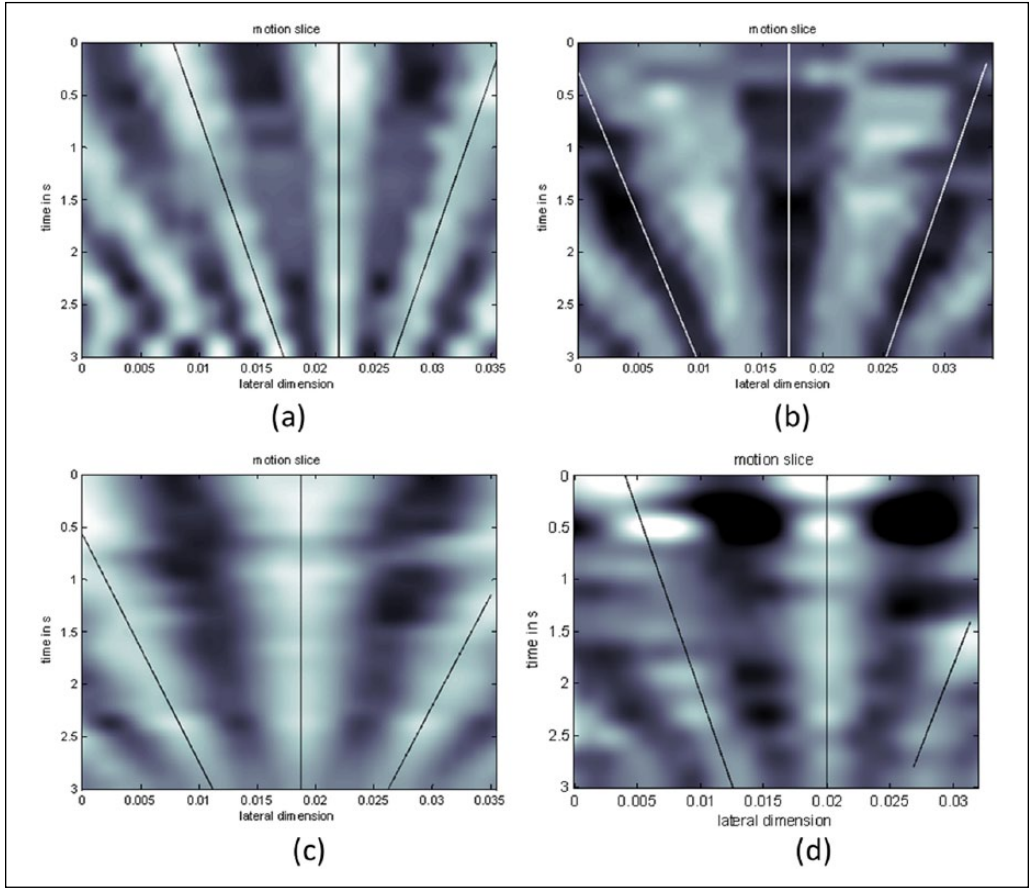
Figure 15. Processed motion slice image for (a) 9.25% gelatin phantom, (b) 13.4% gelatin phantom, (c) 18.5% castor oil phantom, and (d) a ex vivo human liver embedded in 9.25% gelatin. The temperature of the measurements were (a) 20°C, (b) 18.5°C, (c) 18°C, and (d) 14°C. The analyzed motion slice produces time-intersect t_0 and center angle θ_0 which are combined to produce shear speed and shear speed dispersion. The measured shear speed is c_0 = 3.09, 4.27, 4.37, and 2.55 m/s and shear speed dispersion is γ = 7.0×10^{-5}, 8.9×10^{-4}, 1.5×10^{-3}, 5.1×10^{-3} m/s/Hz for (a), (b), (c), and (d), respectively. Higher dispersive values are consistent with lossy oil or fat accumulation.

is limited to specimens and phantoms that can be accessed from parallel sides. In vivo work generally requires surface sources, and the crawling wave patterns from these spread with depth and require a depth-dependent analysis[14] for any estimation scheme.

Finally, we note that this approach assumes a homogeneous material within the ROI to estimate the shear speed and dispersion parameters. Other techniques that use crawling waves in tissues have been derived to produce local estimates of shear speed at a single frequency, with applications to cancer detection and imaging of lesions.[16,17]

Acknowledgment

Declaration of Conflicting Interests

Funding

References

1. Parker KJ, Doyley MM, Rubens DJ. Imaging the elastic properties of tissue: the 20 year perspective. Phys Med Biol. 2011;56:R1-29.
2. Doyley MM. Model-based elastography: a survey of approaches to the inverse elasticity problem. Phys Med Biol. 2012;57:R35-73.
3. Barry CT, Hah Z, Partin A, Mooney RA, Chuang KH, Augustine A, et al. Mouse liver dispersion for the diagnosis of early-stage fatty liver disease: a 70-sample study. Ultrasound Med Biol. 2014;40: 704-13.
4. Parker KJ, Baddour N. The Gaussian shear wave in a dispersive medium. Ultrasound Med Biol. 2014;40:675-84.
5. Barry CT, Mills B, Hah Z, Mooney RA, Ryan CK, Rubens DJ, et al. Shear wave dispersion measures liver steatosis. Ultrasound Med Biol. 2012;38:175-82.
6. Chen S, Fatemi M, Greenleaf JF. Quantifying elasticity and viscosity from measurement of shear wave speed dispersion. J Acoust Soc Am. 2004;115:2781-5.
7. Carstensen EL, Parker KJ, Lerner RM. Elastography in the management of liver disease. Ultrasound Med Biol. 2008;34:1535-46.
8. Carstensen EL, Parker KJ. Physical models of tissue in shear fields. Ultrasound Med Biol. 2014;40: 655-74.
9. Tanter M, Bercoff J, Athanasiou A, Deffieux T, Gennisson JL, Montaldo G, et al. Quantitative assessment of breast lesion viscoelasticity: initial clinical results using supersonic shear imaging. Ultrasound Med Biol. 2008;34:1373-86.
10. Muller M, Gennisson JL, Deffieux T, Tanter M, Fink M. Quantitative viscoelasticity mapping of human liver using supersonic shear imaging: preliminary in vivo feasibility study. Ultrasound Med Biol. 2009;35:219-29.
11. Chen S, Urban MW, Pislaru C, Kinnick R, Zheng Y, Yao A, et al. Shearwave dispersion ultrasound vibrometry (SDUV) for measuring tissue elasticity and viscosity. IEEE Trans Ultrason Ferroelectr Freq Control. 2009;56:55-62.
12. Hoyt K, Castaneda B, Parker KJ (eds). Muscle tissue characterization using quantitative sonoelastography: preliminary results. In: IEEE Ultrasonics Symposium, New York, NY, 28-31 October 2007, pp. 28-31.
13. Orescanin M, Insana M. Shear modulus estimation with vibrating needle stimulation. IEEE Trans Ultrason Ferroelectr Freq Control. 2010;57:1358-67.
14. Partin A, Hah Z, Barry CT, Rubens DJ, Parker KJ. Elasticity estimates from images of crawling waves generated by miniature surface sources. Ultrasound Med Biol. 2014;40:685-94.
15. Hah Z, Hazard C, Mills B, Barry C, Rubens D, Parker K. Integration of crawling waves in an ultrasound imaging system. Part 2: signal processing and applications. Ultrasound Med Biol. 2012;38:312-23.
16. Hoyt K, Castaneda B, Parker KJ. Two-dimensional sonoelastographic shear velocity imaging. Ultrasound Med Biol. 2008;34:276-88.
17. An L, Mills B, Hah Z, Mao S, Yao J, Joseph J, et al. Crawling wave detection of prostate cancer: preliminary in vitro results. Med Phys. 2011;38:2563-72.